REPORT DOCUMENTATION PAGE

Form Approved
OMB No. 0704-0188

1. REPORT DATE *(DD-MM-YYYY)*	**2. REPORT TYPE**	**3. DATES COVERED** *(From - To)*
19-06-2007	Technical Paper	1 July 2005 – 1 July 2007

4. TITLE AND SUBTITLE

On the design of SAR apertures using the Cramer-Rao Bound

5a. CONTRACT NUMBER

5b. GRANT NUMBER

5c. PROGRAM ELEMENT NUMBER
61102F

6. AUTHOR(S)

Robert, Linnehan, David Bready, John K. Schindler, Leonid Perlovsky, Muralidhar Rangaswamy

5d. PROJECT NUMBER
2311

5e. TASK NUMBER
HE

5f. WORK UNIT NUMBER
01

7. PERFORMING ORGANIZATION NAME(S) AND ADDRESS(ES)
AFRL/SNHE
80 Scott Drive
Hanscom AFB MA 01731-2909

8. PERFORMING ORGANIZATION REPORT

9. SPONSORING / MONITORING AGENCY NAME(S) AND ADDRESS(ES)
Electromagnetics Technology Division Source Code 437890
Sensors Directorate
Air Force Research Laboratory
80 Scott Drive
Hanscom AFB MA 01731-2909

10. SPONSOR/MONITOR'S ACRONYM(S)
AFRL-SN-HS

11. SPONSOR/MONITOR'S REPORT NUMBER(S)
AFRL-SN-HS-TP-2007-0002

12. DISTRIBUTION / AVAILABILITY STATEMENT
Approved for public release; distribution unlimited

13. SUPPLEMENTARY NOTES
ESC Clearance Number: 05-0017. Published: IEEE Transactions on Aerospace and Electronic Systems, Vol. 43, No. 1, January 2007

14. ABSTRACT

The Cram´er-Rao inequality is applied to the likelihood function of the synthetic aperture radar (SAR) scatterer parameter vector to relate the choice of flight path to estimation performance. Estimation error bounds for the scatterer parameter vector (including height) are developed for multi-dimensional synthetic apertures, and quantify the performance enhancement over a limited sector of the image plane relative to standard-aperture single-pass SAR missions. An efficient means for the design and analysis of SAR waveforms and flight paths is proposed using simulated scattering models that are limited in size. Comparison of the error bounds to those for standard-aperture SAR show that estimates of scatterer range and cross-range positions are accurate for multi-dimensional aperture SAR, even with the additional estimator for height. Furthermore, multi-dimensional SAR is shown to address the layover problem.

15. SUBJECT TERMS
Cramer-Rao Bounds, synthetic aperture radar, SAR, multi-dimensional apertures

16. SECURITY CLASSIFICATION OF:			**17.LIMITATION OF ABSTRACT**	**18.NUMBER OF PAGES**	**19a. NAME OF RESPONSIBLE PERSON**
a. REPORT	**b. ABSTRACT**	**c.THIS PAGE**			Leonid Perlovsky
Unclassified	Unclassified	Unclassified	UU	13	**19b. TELEPHONE NUMBER** *(include area code)* N/A

Standard Form 298 (Rev. 8-98)
Prescribed by ANSI Std. Z39.18

On the Design of SAR Apertures using the Cramér-Rao Bound

ROBERT LINNEHAN, Student Member, IEEE
Air Force Research Laboratory

DAVID BRADY, Member, IEEE
Northeastern University

JOHN SCHINDLER, Fellow, IEEE
Anteon Corporation

LEONID PERLOVSKY, Senior Member, IEEE

MURALIDHAR RANGASWAMY, Fellow, IEEE
Air Force Research Laboratory

The Cramér-Rao inequality is applied to the likelihood function of the synthetic aperture radar (SAR) scatterer parameter vector to relate the choice of flight path to estimation performance. Estimation error bounds for the scatterer parameter vector (including height) are developed for multi-dimensional synthetic apertures, and quantify the performance enhancement over a limited sector of the image plane relative to standard-aperture single-pass SAR missions. An efficient means for the design and analysis of SAR waveforms and flight paths is proposed using simulated scattering models that are limited in size. Comparison of the error bounds to those for standard-aperture SAR show that estimates of scatterer range and cross-range positions are accurate for multi-dimensional aperture SAR, even with the additional estimator for height. Furthermore, multi-dimensional SAR is shown to address the layover problem.

Manuscript received September 21, 2005; revised April 4, 2006; released for publication May 25, 2006.

IEEE Log No. T-AES/43/1/895039.

Refereeing of this contribution was handled by V. C. Chen.

This work was supported in part by the AFOSR.

Authors' addresses: R. Linnehan, L. Perlovsky, and M. Rangaswamy, Air Force Research Laboratory, Sensors Directorate, 80 Scott Dr., Hanscom AFB, MA 01731-2909, E-mail: (robert.linnehan@hanscom.af.mil); D. Brady, Dept. of Electrical and Computer Engineering, Northeastern University, Boston, MA; J. Schindler, Anteon Corporation, Hanscom AFB, MA.

I. INTRODUCTION

Designs for enhanced resolution of synthetic aperture radar (SAR) systems have been addressed in many ways. In [1], the design of a microstrip antenna architecture was considered for spaced-based SAR applications. In [2], an innovative Cassegrain antenna was shown to improve system performance for space-based SAR systems. In [3], the authors proposed SAR enhancement by introducing a three-dimensional modular filtering architecture in the preprocessing step. In [4], SAR system performance was improved by the joint specification and design of the SAR system and platform. Many other approaches to improving SAR performance have been considered, including digital filtering [5], searching by parallel supercomputers [6], and classification by support vector machines [7].

To date, little work has been published which approaches SAR enhancement via aperture adjustment. Standard SAR employs a 1-D aperture (a synthetic linear array) and assumes a nominal flat ground when processing 2-D range/cross-range images. This removes the range/height ambiguity simply by not estimating height, resulting in the so-called layover problem [8, 9]. In [9] and [10] the layover problem is thoroughly addressed using cross-track, multibaseline SAR interferometry. In a sense, this is an aperture adjustment, requiring the use of multiple antennas, multiple platforms, or multiple passes. Reference [11] describes a technique where a curved flight path with sufficient angular diversity creates a stereo pair in spotlight mode that is then used to measure scatterer height and resolve layover. This too is an aperture adjustment that provides vertical excursion of the radar platform for scatterer height estimation. By contrast, we examine the performance of nonlinear flight paths forming 2-D apertures (sparse synthetic planar arrays) that decouple the range/height ambiguity, resolving the layover problem while providing the potential for 3-D imagery. Unlike interferometry, this can be done using single-pass, monostatic SAR without making multiple data collections. Cramér-Rao bounds (CRBs) do not depend on the methods or techniques to process the observation, hence the design is not restricted to splitting data into stereoscopic components or spotlighting. In this work we also examine a 3-D synthetic aperture where excursions in the range and height dimensions can further decouple the range/height ambiguity and improve overall performance.

Previous literature describes the use of CRBs for radar parametric estimation techniques. In [9] and [12], the authors derive CRBs for the interferometric

phases to evaluate phase estimation techniques. In [13], the author computes bounds for various target parameters, including amplitude, phase and spatial angle. In [14], CRBs are used to evaluate spectral estimation methods applied to curvilinear SAR. In this work we consider the joint estimation problem, and compute the CRBs for all parameters given any aperture that is synthesized. We illustrate that the CRB provides a computationally efficient means to quantify the influence of SAR waveforms, flight paths, and scattering models on the parameter estimation problem. In Section II we introduce the SAR signal and scattering models used in simulations. Section III depicts a mathematical method for computing the CRBs. In Section IV we describe experimental simulations that use bounds to compare standard SAR with multi-dimensional aperture SAR. Finally, conclusions and future directions of the research are offered in Section V.

II. SCATTERING AND SIGNAL MODELS

In this work we consider a finite number of scatterers positioned on a 2-D grid. The centroid of this grid defines the origin of an (x,y,h) Cartesian coordinate system, with the grid lying in the (x,y) plane. Scatterer n is located at cross-range x_n, range y_n, and height h_n, and at time t the radar platform is located at $(x_{\rm ac}(t),y_{\rm ac}(t),h_{\rm ac}(t))$. For the special case of a 1-D aperture, both $y_{\rm ac}$ and $h_{\rm ac}$ would be constants, but for general 3-D apertures all three parameters are functions of t. Fig. 1 illustrates this coordinate system.

For each time-frequency sample index (t,ω_k), with $t \in \{1,2,\ldots,N_t\}$ and $k \in \{1,2,\ldots,N_k\}$ the noiseless received signal $s(t,k)$ is given by

$$e^{j\omega_k t}\cdot s(t,k) = e^{j\omega_k t}\cdot \sum_{n=1}^{N} |a_n| g_n(t,k)$$

$$g_n(t,k) = \frac{1}{R_n^2(t)} e^{j(\phi_n - \beta_k 2R_n(t))} \tag{1}$$

$$R_n(t) = \sqrt{\Delta x_n^2(t) + \Delta y_n^2(t) + \Delta h_n^2(t)}$$

where $\Delta x_n(t) = x_n - x_{\rm ac}(t)$, $\Delta y_n(t) = y_n - y_{\rm ac}(t)$, and $\Delta h_n(t) = h_n - h_{\rm ac}(t)$. Here the summation is over the N scatterers, $R_n(t)$ is the range from the radar to scatterer n at time t, and β_k is the wavenumber for frequency ω_k. The complex reflectivity of scatterer n is a_n, with magnitude $|a_n|$ and phase ϕ_n. We disregard the leading factors in the first line of (1) in the sequel, as they are known to the receiver, and the distribution of the additive noise is invariant to these rotations. In SAR nomenclature, t indexes the slow-time

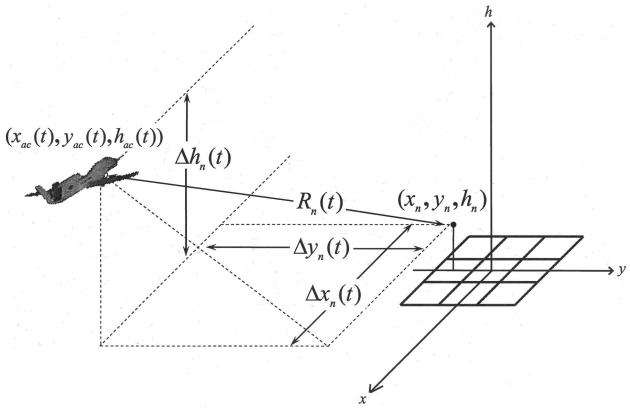

Fig. 1. Illustration of coordinate system used in this work. Radar platform is at position $(x_{\rm ac}(t),y_{\rm ac}(t),h_{\rm ac}(t))$ relative to centroid of 2-D scatterer grid on (x,y)-plane. For the case of standard SAR 1-D aperture, $y_{\rm ac}$ and $h_{\rm ac}$ are constants.

positions over the synthetic array and k indexes the frequency components that synthesize the emitted pulse in fast-time [17]. Although in practice a_n is frequency and aspect angle dependent, we assume constant, isotropic scattering throughout this work.

The observation model is

$$r(t,k) = s(t,k) + n(t,k) \tag{2}$$

where the set $\{n(t,k)\}$ is comprised of independent and identically distributed complex circular Gaussian random variables.

We adopt the following vector notation

$$\begin{aligned}
\mathbf{r} &= [r(1,1)\ldots r(1,N_k)\ldots r(N_t,1)\ldots r(N_t,N_k)]^{\rm T}\\
\mathbf{g}_n &= [g_n(1,1)\ldots g_n(1,N_k)\ldots g_n(N_t,1)\ldots g_n(N_t,N_k)]^{\rm T}\\
\mathbf{G} &= [\mathbf{g}_1\ldots\mathbf{g}_N]\\
\mathbf{a} &= [|a_1|\ldots|a_N|]^{\rm T}.
\end{aligned} \tag{3}$$

The signal and noise vectors, $\mathbf{s}$ and $\mathbf{n}$, are similarly defined. With this notation, the observation vector may be represented as

$$\begin{aligned}
\mathbf{r} &= \mathbf{s} + \mathbf{n}\\
&= \mathbf{G}\mathbf{a} + \mathbf{n}.
\end{aligned} \tag{4}$$

III. CRB DERIVATION

The CRB proceeds from the development of maximum likelihood estimation (MLE) [18]. The effectiveness of the maximum likelihood procedure is revealed by computing the variance of the estimate, a task frequently difficult to perform [19]. However, a lower bound on the variance is often easier to compute using CRB. The result not only applies

to MLE but is in fact valid for any unbiased or asymptotically unbiased estimator.

For a vector of unknown parameters $\boldsymbol{\theta}$, CRB establishes a lower bound on the error covariance matrix of unbiased estimates of $\boldsymbol{\theta}$ [18]. The error covariance matrix $\mathbf{C}$ for the estimator $\hat{\boldsymbol{\theta}}$ is bounded by the inverse of the Fisher information matrix (FIM) $\mathbf{J}$,

$$\mathbf{C} = E\{[\hat{\boldsymbol{\theta}} - \boldsymbol{\theta}][\hat{\boldsymbol{\theta}} - \boldsymbol{\theta}]^{\mathrm{T}}\} \geq \mathbf{J}^{-1} \tag{5}$$

where $E\{\ldots\}$ is the expectation operator, and the inequality is to be interpreted in the positive-definite sense. The (i,j)th element of $\mathbf{J}$ is computed by averaging a second-order mixed partial derivative of the log-likelihood function ℓ,

$$J_{ij} = E\left\{-\frac{\partial^2}{\partial\theta_i\partial\theta_j}\ell\right\}. \tag{6}$$

The ith diagonal element of $\mathbf{J}$ is known as the Fisher information for the parameter θ_i. The off-diagonal elements of $\mathbf{J}$, when $i \neq j$, is called the cross-information between the parameters θ_i and θ_j. Given statistical independence of the white noise components, their joint probability density function has the circular-complex Gaussian form [20] yielding the likelihood function of the received signal

$$f(\mathbf{r} \mid \mathbf{s}) = \frac{1}{(\pi\sigma_0^2)^{N_t N_k}} e^{-(1/\sigma_0^2)(\mathbf{r}-\mathbf{s})^{\mathrm{H}}(\mathbf{r}-\mathbf{s})} \tag{7}$$

where H in the exponent indicates the Hermitian (conjugate transpose) of the column vector, and $\sigma_0^2/2$ is the variance of each in-phase and quadrature white noise term.

Components of the FIM follow directly from the Gaussian form of the likelihood function and the well-known Slepian-Bangs formula [21]. We may concisely present these results if we define

$$\boldsymbol{\Upsilon}_{v_n} = \mathrm{diag}\left[\frac{\Delta v_n(1)}{R_n(1)}\beta_1 \quad \frac{\Delta v_n(1)}{R_n(1)}\beta_2 \cdots \frac{\Delta v_n(1)}{R_n(1)}\beta_{N_k} \quad \frac{\Delta v_n(2)}{R_n(2)}\beta_1 \cdots \frac{\Delta v_n(N_t)}{R_n(N_t)}\beta_{N_k}\right] \tag{8}$$

where v assumes the parameters x, y, or h. We make the following approximation

$$\frac{\partial s(t,k)}{\partial v_n} \approx -j\frac{2\beta_k|a_n|}{R_n(t)}\Delta v_n(t) g_n(t,k) \tag{9}$$

which follows since the derivatives $\partial R_n^{-2}(t)/\partial v_n$ are relatively small in magnitude for all t.

Below denote v and w as two distinct positional parameters x, y, or h, and ℓ is the natural log of the likelihood function in 7. The Slepian-Bangs formula yields the following FIM components:

$$\begin{aligned}
E\left\{-\frac{\partial^2\ell}{\partial|a_n|\partial|a_m|}\right\} &= \frac{2}{\sigma_0^2}\mathrm{Re}\{\mathbf{g}_m^{\mathrm{H}}\mathbf{g}_n\} \\
E\left\{-\frac{\partial^2\ell}{\partial|a_n|\partial v_n}\right\} &= 0 \\
E\left\{-\frac{\partial^2\ell}{\partial|a_n|\partial v_m}\right\} &= \frac{4|a_m|}{\sigma_0^2}\mathrm{Im}\{\mathbf{g}_n^{\mathrm{H}}\boldsymbol{\Upsilon}_{v_m}\mathbf{g}_m\} \qquad \text{for} \quad m \neq n \\
E\left\{-\frac{\partial^2\ell}{\partial v_n^2}\right\} &= \frac{8|a_n|^2}{\sigma_0^2}\mathbf{g}_n^{\mathrm{H}}\boldsymbol{\Upsilon}_{v_n}\boldsymbol{\Upsilon}_{v_n}\mathbf{g}_n \\
E\left\{-\frac{\partial^2\ell}{\partial v_n\partial w_n}\right\} &= \frac{8|a_n|^2}{\sigma_0^2}\mathbf{g}_n^{\mathrm{H}}\boldsymbol{\Upsilon}_{v_n}\boldsymbol{\Upsilon}_{w_n}\mathbf{g}_n \\
E\left\{-\frac{\partial^2\ell}{\partial v_n\partial w_m}\right\} &= \frac{8|a_n||a_m|}{\sigma_0^2}\mathrm{Re}\{\mathbf{g}_n^{\mathrm{H}}\boldsymbol{\Upsilon}_{v_n}\boldsymbol{\Upsilon}_{w_m}\mathbf{g}_m\} \\
E\left\{-\frac{\partial^2\ell}{\partial\phi_n\partial\phi_m}\right\} &= \frac{2|a_n||a_m|}{\sigma_0^2}\mathrm{Re}\{\mathbf{g}_n^{\mathrm{H}}\mathbf{g}_m\} \\
E\left\{-\frac{\partial^2\ell}{\partial\phi_n\partial|a_n|}\right\} &= 0 \\
E\left\{-\frac{\partial^2\ell}{\partial\phi_n\partial|a_m|}\right\} &= -\frac{2|a_n|}{\sigma_0^2}\mathrm{Im}\{\mathbf{g}_n^{\mathrm{H}}\mathbf{g}_m\} \qquad \text{for} \quad m \neq n \\
E\left\{-\frac{\partial^2\ell}{\partial\phi_n\partial v_m}\right\} &= -\frac{4|a_n||a_m|}{\sigma_0^2}\mathrm{Re}\{\mathbf{g}_n^{\mathrm{H}}\boldsymbol{\Upsilon}_{v_m}\mathbf{g}_m\}.
\end{aligned} \tag{10}$$

Fisher information for the uniformly distributed random phases ϕ_n of each scatterer are computed but treated as nuisance parameters. It was shown by Gini [22] that assuming knowledge of a parameter and excluding it in the FIM lowers, or at least has no affect on, the variance bounds for the remaining parameters. In this sense, the CRBs for the parameters of interest are larger when the random phases are considered unknown and included in $\mathbf{J}$.

A compact description of the FIM for SAR is achievable by defining

$$\begin{aligned}
\tilde{\mathbf{v}}_n &= 2|a_n|\boldsymbol{\Upsilon}_{v_n}\mathbf{g}_n \\
\mathbf{V} &= [\tilde{\mathbf{v}}_1 \quad \tilde{\mathbf{v}}_2 \ldots \tilde{\mathbf{v}}_N]
\end{aligned} \tag{11}$$

where $\tilde{\mathbf{v}}_n$ can be $\tilde{\mathbf{x}}_n$, $\tilde{\mathbf{y}}_n$ or $\tilde{\mathbf{h}}_n$, and $\mathbf{V}$ can be $\mathbf{X}$, $\mathbf{Y}$ or $\mathbf{H}$. Also, we define

$$\boldsymbol{\Phi} = -[|a_1|\mathbf{g}_1 \quad |a_2|\mathbf{g}_2 \ldots |a_N|\mathbf{g}_N] \tag{12}$$

and construct the block matrix

$$\mathbf{M} = [\mathbf{X} \quad \mathbf{Y} \quad \mathbf{H} \quad \boldsymbol{\Phi}]. \tag{13}$$

Fisher information and cross-information among the scattering positions and phases are given by the matrix

$$\mathbf{J}_{xyh\phi} = \frac{2}{\sigma_0^2}\mathrm{Re}\{\mathbf{M}^{\mathrm{H}}\mathbf{M}\}. \tag{14}$$

The matrix containing information of scattering magnitudes is

$$\mathbf{J}_{|a|} = \frac{2}{\sigma_0^2}\mathrm{Re}\{\mathbf{G}^{\mathrm{H}}\mathbf{G}\}. \tag{15}$$

Finally, the matrix $\mathbf{P}$ yields cross-information among the scattering magnitudes and positions and is of dimensions $4N \times N$

$$\mathbf{P} = \frac{2}{\sigma_0^2}\mathrm{Im}\{\mathbf{M}^{\mathrm{H}}\mathbf{G}\}. \tag{16}$$

The complete FIM for SAR has order $5N$ and the following form

$$\mathbf{J} = \begin{bmatrix} \mathbf{J}_{xyh\phi} & \mathbf{P} \\ \mathbf{P}^{\mathrm{T}} & \mathbf{J}_{|a|} \end{bmatrix}. \tag{17}$$

The CRBs for each scatterer are on the diagonal of $\mathbf{J}^{-1}$ in the form

$$\mathrm{diag}(\mathbf{J}^{-1}) = [\mathrm{CRB}_{x_1}\ \mathrm{CRB}_{x_2} \ldots \mathrm{CRB}_{x_N} \mathrm{CRB}_{y_1} \ldots \mathrm{CRB}_{y_N} \ldots \mathrm{CRB}_{h_N} \ldots \mathrm{CRB}_{\phi_N} \ldots \mathrm{CRB}_{|a_N|}] \tag{18}$$

where CRB_{q_n} denotes the CRB for parameter q for the nth scatterer.

IV. MULTI-DIMENSIONAL APERTURES

The following subsections describe a computationally efficient method of simulating a SAR process in order to compute CRBs on the scattering parameters of interest. First we describe a way to greatly reduce the number of scatterers modeled around one scatterer of interest so the effects of clutter may be examined. We then describe a method to undersample the aperture and the transmitted waveform, while averting the effects of grating lobes. The resulting simulation is used to evaluate the legitimacy of multi-dimensional apertures and compare performance with standard SAR processing.

A. Minimized Scattering Model

In this paper we emphasize Ku-band SAR which might be used on an agile unmanned air vehicle (UAV) to produce high resolution images. The radar is assigned the following parameters:

center frequency	$f_c = 16.7$ GHz
bandwidth	$B = 1.67$ GHz
synthetic aperture	$L = 1176$ m
aircraft velocity	$v_{\mathrm{ac}} = 56$ m/s
aircraft height	$h_{\mathrm{ac}} = 3000$ m
nominal range to target	$R_0 = 6708$ m

Based on these values, approximate resolution in range and azimuth are, respectively, [17]

$$\delta_r \approx \frac{c}{2B} = 0.090 \text{ m}, \qquad \delta_a \approx \frac{\lambda R_0}{2L} = 0.051 \text{ m} \tag{19}$$

where c is the speed of light.

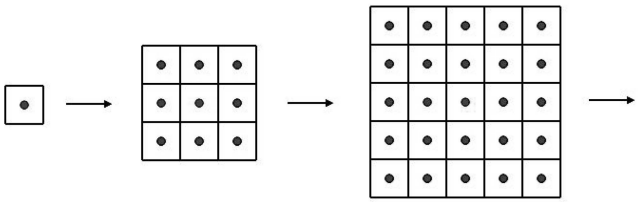

Fig. 2. With the target center located, we increase grid size and examine effects additional scatterers have on its CRB. CRB asymptotes and minimal number of scatterers N used to replicate clutter around target is determined.

Typical SAR processing estimates scattering amplitudes for predetermined locations on a large patch of ground. The number of estimated positions of the ground patch depends on the pixel size desired by the operator. Generally speaking, pixel dimensions are based on the resolution in range and cross-range provided by the radar. The image of a large swath could include millions of scattering measurements. Thus in many cases the large computational requirements necessitates off-line formation of the high-resolution images.

Jointly computing the CRBs for parameters x_n, y_n, h_n, $|a_n|$ and the nuisance parameter ϕ_n of a single scatterer involves the inversion of a 5×5 matrix $\mathbf{J}$. Although a telling exercise, it may be more informative to observe lower error bounds for many scattering elements within the desired ground patch. Thorough analysis of a radar system or the design of a new system would entail computing CRBs for millions of scatterers, not just one, i.e., observing how surrounding clutter affects the CRBs. However, constructing and inverting such a large FIM is not feasible using a desktop computer for analysis.

One method to overcome this complexity is to simply surround a scatterer of interest, hereafter known as the target, with just enough scatterers to approach the effects of an infinitely large area of clutter and yet small enough to limit the size of $\mathbf{J}$. The number of scatterers needed to meet these criteria depends, among other things, on the spacing among the scatterers and their strength relative to the targets, i.e., the signal-to-clutter ratio (SCR). This number is determined by computing the CRB for the target alone and examining the increase in this bound as the number of surrounding scatterers increases. At some point the additional clutter no longer influences the CRBs of the target and an asymptote is reached. We start by computing the CRB on estimating $|a_n|$ for the target only. Then we increase the number of cells to a 3×3 grid and compute the CRB on estimating $|a_n|$ for all $N = 9$ scatterers. Then we increase the cells to a 5×5 grid, and then to a 7×7 and so on (see Fig. 2), computing CRBs for all scatterers.

Fig. 3 shows the CRB for only the target magnitude as the grid size increase. Spacing among

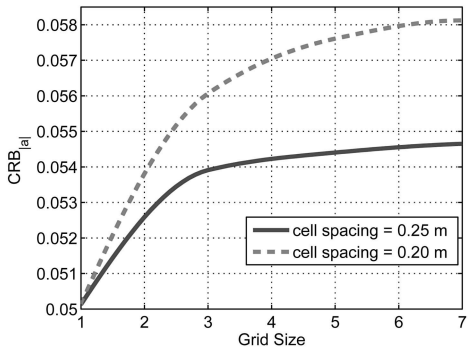

Fig. 3. Bound for reflectivity, $\mathrm{CRB}_{|a|}$, is seen to asymptote as number of scatterers increases (depending on scatterer density).

the cells is tried at 0.20 m and at 0.25 m. We can see the bound approaches an asymptote at about the 3×3 grid size for the larger spacing, and at about the 7×7 when the scatterers are more closely spaced. The difference indicates that target parameters are more difficult to resolve when the surrounding scatterers are closer together. For simulations where the effects of clutter are examined we will construct a 3×3 or 7×7 depending on the average spacing among the scatterers. This will create a clutter patch large enough to replicate an infinitely large area around the target. The target will likely have the largest CRBs since it is located among the most dense clutter. Influence from surrounding scatterers on the target parameter estimates is inversely proportional to their distance from the target [16].

B. Undersampled Aperture and Chirp

Typical pulse repetition frequencies (PRF) of Ku-band SAR are on the order of 1 kHz requiring tens of thousands of pulses to achieve the desired resolution. However, in our simulations we show that the PRF can be substantially reduced. Although the undersampled, or sparse, aperture causes quasi-grating lobes in the azimuth dimension, these will not impair the analysis if they are physically beyond the region of interest. The sampling rate of the linear FM pulse can also be reduced to further ease computational complexity. The pulse sampling rate is minimized while assuring that quasi-grating lobes in range dimension are beyond the geometric limits of the scattering model ($\pm \sim 0.75$ m). Fig. 4 shows the magnitude response of the white noise matched filter in the azimuth (a) and range (b) dimensions (given the operational parameters mentioned above) with a PRF of 2 pulses/s and a frequency sampling period of 100 MHz. The first quasi-grating lobes are well beyond the clutter swath used in the simulations.

The signal-to-noise ratio (SNR) accumulated over the aperture is selected to be 10 dB. The noise power is appropriately scaled based on the amount of data

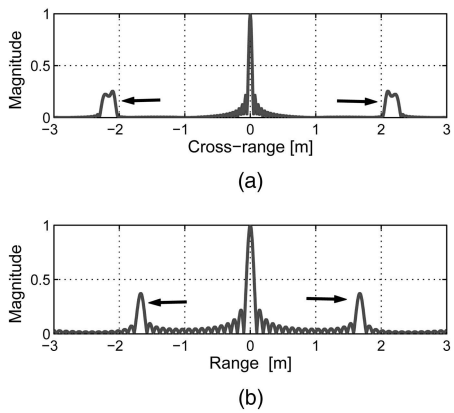

Fig. 4. Magnitude response in cross-range and range dimensions with first quasi-grating lobes indicated by arrows. Reducing the PRF to 2 pulses/s and sampling the pulse every 100 MHz positions the grating lobes beyond the region of interest in this experiment.

collected and the range to target at broadside,

$$\sigma_0^2 = \frac{N_t N_k}{\mathrm{SNR} \cdot R_0^4}. \tag{20}$$

C. Vertical Aperture

Standard SAR range resolution is achieved by narrowing an uncompressed received pulse that has sufficient bandwidth. Resolution in cross-range is achieved with a narrow beamwidth produced over the synthetic aperture created by linear cross-range motion. However, as would be expected, introducing height estimation results in an ill-conditioned matrix $\mathbf{J}$ if some aperture in the vertical dimension is not included. This is intuitively known and mathematically satisfied by examining the matrix $\mathbf{J}_{xyh}$ for a single scatterer,

$$\mathbf{J}_{xyh} = \frac{2}{\sigma_0^2} \begin{bmatrix} \tilde{\mathbf{x}}_1^{\mathrm{H}} \tilde{\mathbf{x}}_1 & \tilde{\mathbf{x}}_1^{\mathrm{H}} \tilde{\mathbf{y}}_1 & \tilde{\mathbf{x}}_1^{\mathrm{H}} \tilde{\mathbf{h}}_1 \\ \tilde{\mathbf{y}}_1^{\mathrm{H}} \tilde{\mathbf{x}}_1 & \tilde{\mathbf{y}}_1^{\mathrm{H}} \tilde{\mathbf{y}}_1 & \tilde{\mathbf{y}}_1^{\mathrm{H}} \tilde{\mathbf{h}}_1 \\ \tilde{\mathbf{h}}_1^{\mathrm{H}} \tilde{\mathbf{x}}_1 & \tilde{\mathbf{h}}_1^{\mathrm{H}} \tilde{\mathbf{y}}_1 & \tilde{\mathbf{h}}_1^{\mathrm{H}} \tilde{\mathbf{h}}_1 \end{bmatrix}. \tag{21}$$

Because Δy_1 and Δh_1 are constants and not a function of t using standard, side-looking SAR, the determinant of (21) is zero. Another way of stating this is the correlation coefficient between $\tilde{\mathbf{y}}_1$ and $\tilde{\mathbf{h}}_1$ is unity,

$$\rho_{yh} = \frac{\tilde{\mathbf{y}}_1^{\mathrm{H}} \tilde{\mathbf{h}}_1}{\sqrt{\tilde{\mathbf{y}}_1^{\mathrm{H}} \tilde{\mathbf{y}}_1 \tilde{\mathbf{h}}_1^{\mathrm{H}} \tilde{\mathbf{h}}_1}} = 1.0. \tag{22}$$

In order to reduce ρ_{yh}, some variation in Δh_1 is required. This might lead one to believe that simply directing the radar platform at some non-zero angle relative to the ground plane will satisfy the requirement of both azimuthal and vertical apertures. Fig. 5 shows a linear flight path adjusted to an angle γ and the radar's position relative to a single scatterer located at ground range Δy. Note here

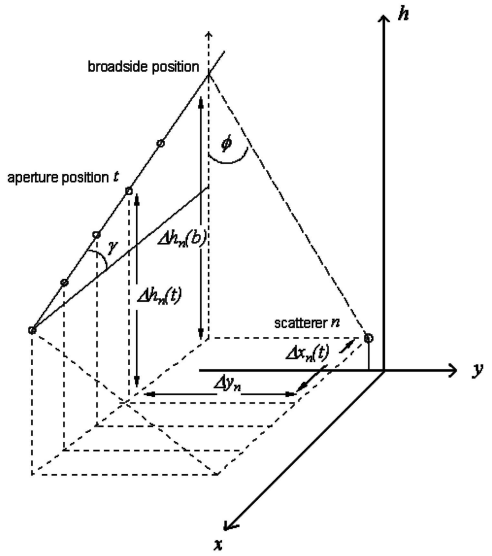

Fig. 5. Linear aperture at angle γ relative to horizon creates singular FIM $\mathbf{J}_{xyh}$. Scatterer height cannot be estimated along with range in this case.

that both Δx and Δh are functions of t. However, further investigation reveals that this FIM is also ill-conditioned. We again examine the block matrix of $\mathbf{J}$ in (21), and since the factors defined for $\tilde{\mathbf{x}}$, $\tilde{\mathbf{y}}$ and $\tilde{\mathbf{h}}$ are identical in the single scatterer case except for the geometric differentials, the matrix can be simplified to

$$\mathbf{J}_{xyh} \sim \begin{bmatrix} \boldsymbol{\Delta}\mathbf{x}_1^{\mathrm{T}}\boldsymbol{\Delta}\mathbf{x}_1 & \boldsymbol{\Delta}\mathbf{x}_1^{\mathrm{T}}\boldsymbol{\Delta}\mathbf{y}_1 & \boldsymbol{\Delta}\mathbf{x}_1^{\mathrm{T}}\boldsymbol{\Delta}\mathbf{h}_1 \\ \boldsymbol{\Delta}\mathbf{y}_1^{\mathrm{T}}\boldsymbol{\Delta}\mathbf{x}_1 & \boldsymbol{\Delta}\mathbf{y}_1^{\mathrm{T}}\boldsymbol{\Delta}\mathbf{y}_1 & \boldsymbol{\Delta}\mathbf{y}_1^{\mathrm{T}}\boldsymbol{\Delta}\mathbf{h}_1 \\ \boldsymbol{\Delta}\mathbf{h}_1^{\mathrm{T}}\boldsymbol{\Delta}\mathbf{x}_1 & \boldsymbol{\Delta}\mathbf{h}_1^{\mathrm{T}}\boldsymbol{\Delta}\mathbf{y}_1 & \boldsymbol{\Delta}\mathbf{h}_1^{\mathrm{T}}\boldsymbol{\Delta}\mathbf{h}_1 \end{bmatrix}. \quad (23)$$

Looking again at Fig. 5 we see that the height above the scatterer at any position t along the array is equal to the current change in height from the original position on the aperture minus the radar height at broadside $h_n(b)$. Thus we can define

$$\tan(\gamma) = \frac{\Delta h_n(t) - \Delta h_n(b)}{\Delta x_n(t)} \quad (24)$$

and

$$\tan(\phi) = \frac{\Delta h_n(b)}{\Delta y_n}. \quad (25)$$

Then the height at any t is

$$\Delta h_n(t) = \tan(\phi)\Delta y_n - \tan(\gamma)\Delta x_n(t). \quad (26)$$

Since γ and ϕ are constants for a linear array, the row and column associated with $\boldsymbol{\Delta}\mathbf{h}_1$ in (23) are linear combinations of the other two rows and columns, yielding a singular matrix of rank 2. Therefore, not only is vertical aperture required for height estimation but some nonlinearity in the aperture formation, offering spatial diversity in a 2-D plane is also needed.

One method of vertical excursion that achieves a 2-D aperture is a sinusoidal flight path, parameterized by spatial amplitude A_{ac}, spatial frequency f_{ac}, and phase relative to its broadside position as

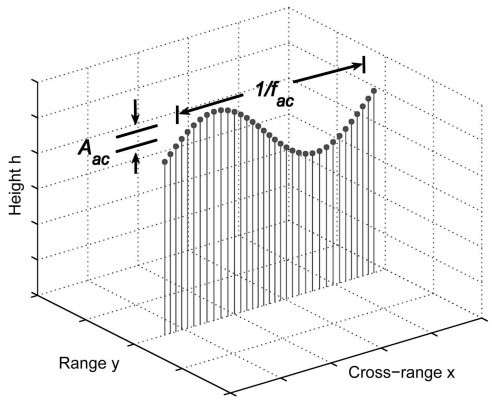

Fig. 6. 2-D aperture in form of sinusoidal flight path parameterized by spatial amplitude A_{ac} and frequency f_{ac}.

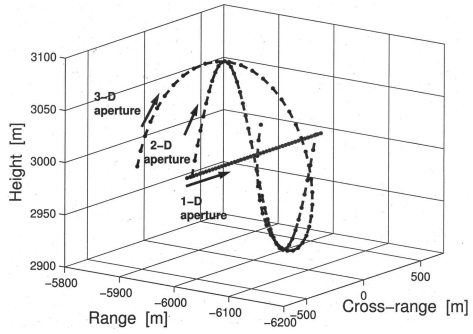

Fig. 7. Examples of flight paths that employ 1-D, 2-D, and 3-D apertures.

demonstrated in Fig. 6. Ultimately the 2-D aperture reduces ρ_{yh} and this lower correlation begins to mitigate the range/height ambiguity, allowing these parameters to be estimated.

For our simulations we try to maintain nearly identical distances between array positions when creating 2-D apertures. This is achieved by determining the separation distance d between array positions based on the PRF and the speed of the aircraft, and using the general formula for computing the arc length of a function $f(x)$ between consecutive positions [23] (see appendix)

$$d = \int_a^b \sqrt{1 + [f'(x)]^2}\,dx. \quad (27)$$

A third dimension included in the aperture further enhances performance relative to the 2-D case. We accomplish this by applying a cosine function to the flight path in the range dimension (see Fig. 7). This is analogous to a 3-D curve traced out by a circularly polarized wave. As a result the correlation coefficients among the geometric parameters, ρ_{yh}, ρ_{xy}, and ρ_{xh} are further decreased, subsequently reducing the CRBs for all parameters of interest.

A question arises as to whether an acceptable ambiguity function is maintained when the synthetic aperture includes additional dimensions. Fig. 8(a)–(c) show the magnitude response for standard 1-D SAR

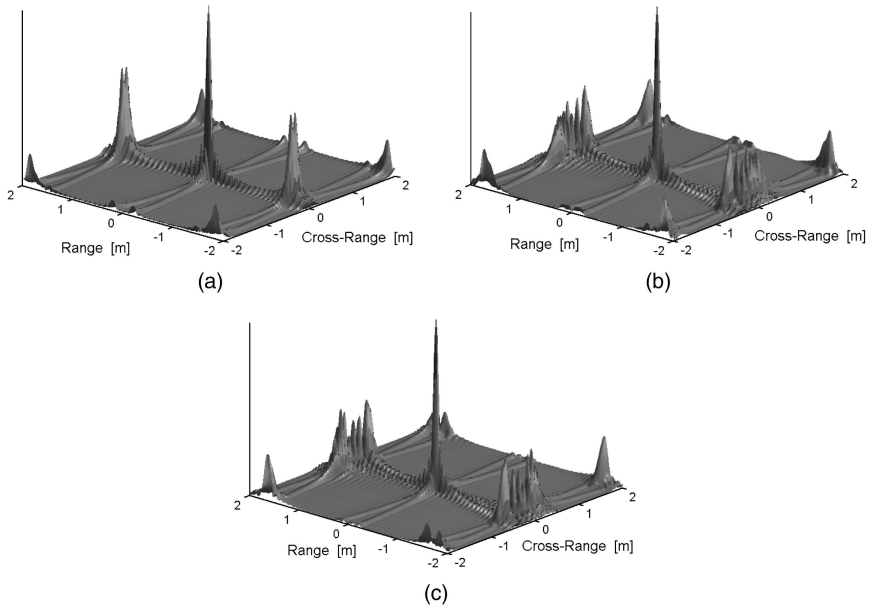

Fig. 8. Ambiguity functions for 1-D, 2-D, 3-D apertures. Mainlobes of multi-dimensional cases retain shape similar to that of standard SAR. (a) Magnitude response for 1-D aperture. (b) Magnitude response for 2-D aperture. (c) Magnitude response for 3-D aperture.

and for the alternate 2-D and 3-D flight paths. It is evident from these plots that the mainlobe of the point spread function sufficiently retains its shape, and the grating lobes are still physically beyond the region of interest.

D. Comparison of CRBs for Multi-Dimensional Apertures

Computations were performed on a 7×7 cell grid (49 scatterers) with the target scatterer having complex reflectivity a_t located at the center. The cells are arranged so that their centers are nominally 0.25 m apart. To avoid any irregularity in the results because of the periodic placement of the scatterers, their positions within each cell is random, uniformly distributed in range and cross-range. The limits on the distribution are 1/4 of the cell spacing so in this case the closest two scatterers can be to one another is 0.125 m. This minimum separation is still greater than the range and azimuth resolutions according to (19). The heights of all the scatterers are Gaussian distributed with mean height 1 m and standard deviation $\sigma_h = 0.125$ m. Finally, the real and imaginary components of scatterer amplitude are randomly generated using independent, standard Gaussian distributions. Because the results are so heavily dependent on the realization, especially the geometric parameters, the average of a series of random realizations is computed in the following experiment. An illustration of one scattering realization is seen in Fig. 9. The experiment compares the CRBs of standard 1-D aperture SAR with those of 2-D and 3-D synthetic apertures. The displayed data are averaged for 200 randomly generated scattering

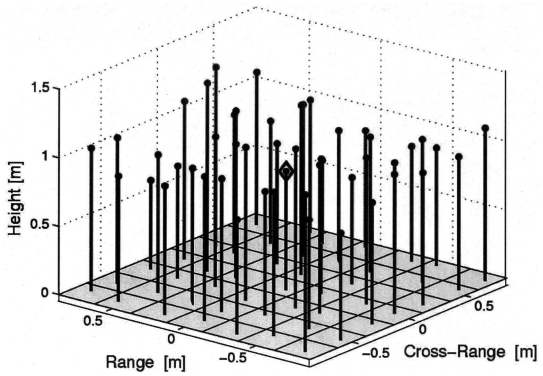

Fig. 9. Scattering model realization with target in center cell (◊), and clutter randomly positioned within surrounding cells.

realizations. The model for standard SAR assumes a linear, side-looking flight path and no height estimation, so from (13) we have

$$\mathbf{M}_{1\text{-D}} = [\mathbf{X} \quad \mathbf{Y} \quad \mathbf{\Phi}]. \tag{28}$$

Excluding $\mathbf{H}$ in the FIM implies that scatterer heights are known for the 1-D aperture case. As stated previously, the processing assumes a nominal flat ground level and thus the CRBs for the remaining parameters should inherently be smaller relative to those of the multi-dimensional aperture cases that do include height estimation.

The number of pulses (total transmitted power) and aircraft velocity is consistent in all three aperture models. The 1-D aperture is slightly longer in azimuth, producing a more narrow beam and thus is expected to have an even lower CRB for cross-range. The accumulated SNR is also equivalent for the three different flight paths, i.e., the average slant range to the target $R_{tg}(t)$ over the array positions at t is

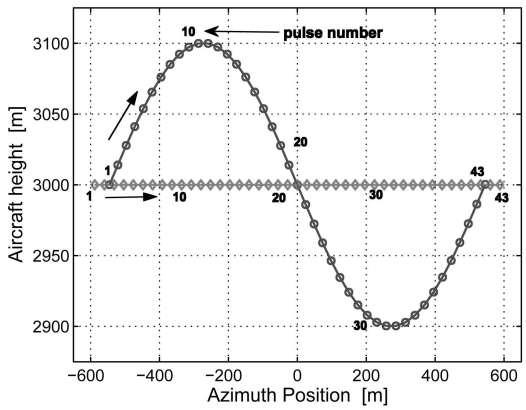

Fig. 10. 1-D (◇) and 2-D aperture (·) labeled with pulse numbers.

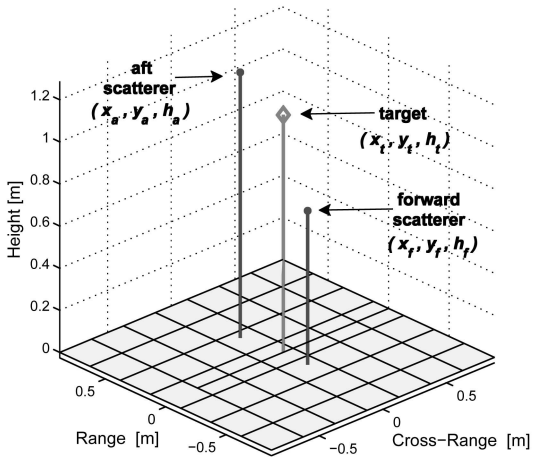

Fig. 11. Target (◇) and a "laid over" forward scatterer that inhibits accurate measurements of both magnitudes.

the same for the three apertures. The 1-D and 2-D apertures are seen in detail in Fig. 10 on geometric axes with array positions indexed by pulse numbers (positions along a 3-D aperture are similarly indexed). Fig. 12(a)–(d) show CRBs for each parameter as a function of pulse number over the synthetic aperture formation, correlating to the pulse numbers seen in the aperture plots of Fig. 10. Log values of the CRBs allow the three curves to be displayed together for comparison. The beginning portions of the apertures do not contain enough data to condition the matrix **J**, and thus displayed CRBs start at pulse number 15.

In Fig. 12(a) the CRB for cross-range target estimation is larger for the 2-D (dashed) and 3-D (dotted) flight paths compared with standard as expected. However, the values for the bounds at the completion of the apertures (43rd pulse) are all on the order of 10^{-4} which is sufficiently small given the radar cross-range resolution. An ancillary observation is the smoothness of the curve for the standard aperture relative to the others. This occurs because the linear aperture exhibits a more consistent data collection process that steadily improves SNR and azimuth resolution. For instance, the 2-D aperture bounds in Fig. 12(a) decrease sharply after pulse 15 through 22, and then remains flat until pulse 35. This corresponds to the geometry in Fig. 10 where the aircraft is not contributing as much to the azimuthal aperture in the center portion of the plot.

Bounds for range estimates are shown in Fig. 12(b). Examining the adequacy of range CRBs we see the standard SAR results in a range CRB of 1.62×10^{-4} m^2, which is clearly acceptable given the resolution of 0.09 m in range. The 2-D aperture offers a range CRB of 3.54×10^{-3} m^2, and thus a 95% confidence interval of 0.119 m. Given that the average spacing among the scatterers in this model is 0.25 m (more than twice the range resolution) this is sufficient to resolve the target in range for any realization. The 3-D aperture yields a notable improvement in the range CRB compared with the 2-D case.

Fig. 12(c) shows the minimum error variance of height estimation for the multi-dimensional apertures only. The results are correlated with the range error variances in Fig. 12(b), scaled by a factor of about 3. Again it appears this bound is reduced by including range excursion in the aperture.

Examining the results in Fig. 12(d) the average magnitude CRB is much worse for the standard SAR case. This is not related to SNR; as stated above the accumulated SNR for the multi-dimensional paths equals that of the linear path. The poor average error variance in amplitude estimates occurs with standard SAR because a small percentage of the random realizations result in layover of the target with an adjacent scatterer. This is worthy of further investigation into a particular realization where the 1-D aperture cannot resolve the target from a nearby scatterer. Fig. 11 shows only the three relevant scatterers for this discussion, the target at position (x_t, y_t, h_t), and the adjacent scatterers directly forward and aft at positions $(x_{\text{fwd}}, y_{\text{fwd}}, h_{\text{fwd}})$ and $(x_{\text{aft}}, y_{\text{aft}}, h_{\text{aft}})$, respectively. The placement of the forward scatterer at a height h_{fwd} happens to have a broadside range, $R_{0,\text{fwd}} = 6707.68$ m within 0.02 m of the target broadside range $R_{0,t} = 6707.70$ m, for all three apertures. Even at the radar positions for the first and last pulses (the beginning and end of the synthetic array), the range to the target and the forward scatterer are within 0.01 m of each other, whereas the aft scatterer maintains about a 0.1 m difference in range. The results from this layover realization of the target CRBs for the three apertures are shown below in Table I.

We see that the the range and cross-range bounds for the 1-D aperture are an order of magnitude worse than those for the 2-D and 3-D case. Estimation of magnitude significantly degenerates for the 1-D aperture since $\text{CRB}_{|a_t|} = 37.16$. The magnitude CRB for the forward scatterer is $\text{CRB}_{|a|,\text{fwd}} = 37.11$, suggesting that the magnitude of these scatterers cannot be resolved, whereas for the aft scatterer $\text{CRB}_{|a|,\text{aft}} = 0.052$, suggesting this adjacent

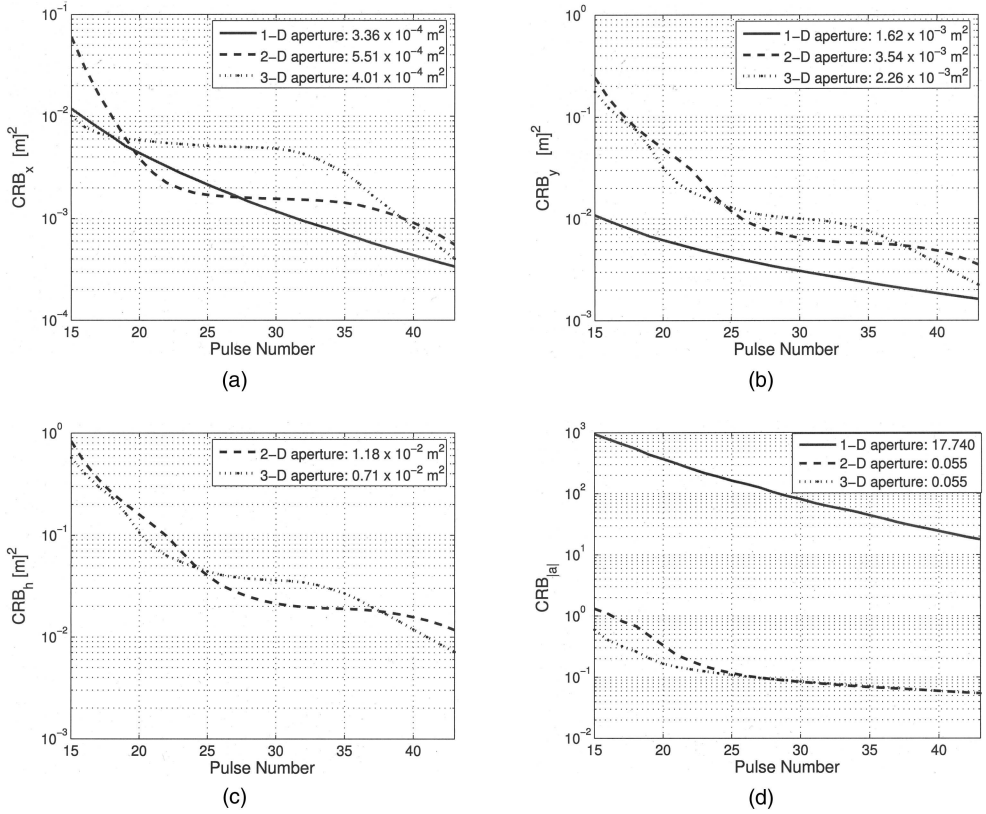

Fig. 12. CRBs over synthetic aperture formation. Label indicates value of bound when aperture is complete. (a) CRBs for cross-range. (b) CRBs for range. (c) CRBs for height. (d) CRBs for magnitude.

TABLE I
Cramér Rao Bounds on Cross-Range, Range, Height and Magnitude Estimates for Various Apertures

Apt.	CRB_{x_t}	CRB_{y_t}	CRB_{h_t}	$\text{CRB}_{\lvert a_t\rvert}$
1-D	7.32×10^{-4}	1.46×10^{-3}	—	37.16
2-D	7.68×10^{-5}	5.24×10^{-4}	1.90×10^{-3}	0.062
3-D	4.67×10^{-5}	2.75×10^{-4}	9.70×10^{-4}	0.062

scatterer is resolvable. The improvement for the multi-dimensional aperture cases occurs because of a decrease in the correlation among a scatterers reflectivity and the surrounding clutter. The correlation coefficient between a scatterer's magnitude and a different scatterer's range is

$$\rho_{y,a} = \text{Im}\left\{ \frac{\tilde{\mathbf{y}}_n^{\text{H}} \mathbf{g}_m}{\sqrt{\tilde{\mathbf{y}}_n^{\text{H}} \tilde{\mathbf{y}}_n \mathbf{g}_m^{\text{H}} \mathbf{g}_m}} \right\} \tag{29}$$

for $n \neq m$. For the 1-D aperture the correlation between the target range and forward scatterer's magnitude is $\rho_{y_t,a_{\text{fwd}}} = 0.51$, whereas the correlation with the aft scatterer is significantly lower, $\rho_{y_t,a_{\text{aft}}} = 0.01$. For the multi-dimensional 2-D and 3-D apertures $\rho_{y_t,a_{\text{fwd}}} = 0.17$ and $\rho_{y_t,a_{\text{fwd}}} = 0.24$, respectively, which is higher than normal but still low enough to not affect the estimators.

Layover may not significantly impact low-resolution SAR images where only approximate locations of large buildings, roads, airstrips or other objects are needed. However, for high resolution images, layover can critically affect analysis if attempting to discern details of a small scene or target. In this case multi-dimensional flight paths, potentially used with spotlight mode SAR, can provide height estimation and improved reflectivity measurements.

V. CONCLUSIONS

In this paper we have described a method of efficiently computing the CRBs for parameters related to image formation based on a signal model for SAR. In particular we compute CRBs for the geometric positions, including height, and magnitude of all scatterers that are modeled. We then use this method to illustrate the potential benefits of multi-dimensional flight paths that permit height estimation and improve imaging performance by resolving scatterers that would layover in range bins of adjacent scatterers using standard SAR processing. The 2-D and 3-D apertures exhibit this improved performance over a limited sector of the image plane.

Further work in this area is to develop methods of optimizing the multi-dimensional apertures using CRBs. A general optimization process would minimize the CRBs with respect to a sinusoidal flight

path parameterized by spatial amplitude, frequency, and phase. Another method would adaptively optimize performance by adjusting the flight path when viewing a particular object or scene.

Future research could include the application of Cramér-Rao theory to tracking moving targets, in particular those below clutter [24]. Another possibility may be to explore the potential of multi-static SAR using CRBs. The results can offer optimal system design for cooperative control of multiple sensor platforms. They can also serve as a reference for evaluating established or developmental processing algorithms.

APPENDIX. MAINTAINING EQUAL ARRAY POSITION SEPARATION FOR A SINUSOIDAL PATH

In general, if f is a smooth function on $[a,b]$, the arc length from a to b is

$$d = \int_a^b \sqrt{1 + [f'(x)]^2}dx. \tag{30}$$

Simulating a sinusoidal aperture with a constant PRF requires equal arc lengths between array positions along the flight path. In our case the height of the aircraft varies sinusoidally as a function of uniform temporal steps, but nonuniform spatial values in x. That is, if we require the arc length to be

$$d = v_{\text{ac}}/\text{PRF} \tag{31}$$

and the aircraft height to be

$$h(x) = h_{\text{ac}} + A_{\text{ac}} \sin(2\pi f_{\text{ac}} x) \tag{32}$$

where h_{ac} is the nominal aircraft altitude, we need to compute values for x_t, $t = 1,\ldots,N_t$ that maintain uniform values of d.

The integral

$$\int_{x_t}^{x_{t+1}} \sqrt{1 + [2\pi f_{\text{ac}} A_{\text{ac}} \cos(2\pi f_{\text{ac}} x)]^2}dx \tag{33}$$

is difficult to evaluate analytically. The discrete version is written

$$d = \sum_{x_t}^{x_{t+1}} \sqrt{1 + [2\pi f_{\text{ac}} A_{\text{ac}} \cos(2\pi f_{\text{ac}} x)]^2}dx$$

$$\text{for} \quad t = 1,\ldots,N_t - 1. \tag{34}$$

Letting dx equal a small fraction of the spatial period, $dx = 0.001/f_{\text{ac}}$, and by initializing $x_1 = 0$, we can numerically find the upper limit x_2 that satisfies (34), and continue this process recursively until $t = N_t - 1$. A spatial phase ϕ_{ac} can also be easily introduced.

REFERENCES

[1] Pokuls, R., Uher, J., and Pozar, D. M.
Microstrip antennas for SAR applications.
IEEE Transactions on Antennas and Propagation, **46**, 9 (1998), 1289–1296.

[2] Tomiyasu, K.
Conceptual reconfigurable antenna for 35 GHz high-resolution spaceborne synthetic aperture radar.
IEEE Transactions on Aerospace and Electronic Systems, **39**, 3 (2003), 1069–1074.

[3] Lim, C. H., and Soon, Y. T.
Real time synthetic aperture radar (SAR) preprocessor design via three-dimensional modular filtering architecture.
In *Proceedings of IEEE International Geoscience and Remote Sensing Symposium*, vol. 1, 1997, 487–489.

[4] Veseky, J. F., and Cornwall, J. M.
Integrated design of synthetic aperture radars for unmanned aircraft.
In *Proceedings of IEEE International Geoscience and Remote Sensing Symposium*, vol. 4, 1996, 2347–2348.

[5] Adams, J. W., Medlin, G. W., and Bayma, R. W.
Digital filters for synthetic aperture radar.
In *Proceedings of IEEE National Radar Conference*, 1988, 171–176.

[6] Holm, S., and Maoy, A.
Integrated design of synthetic aperture radars for unmanned aircraft.
In *Proceedings of International Conference on Acoustics, Speech and Signal Processing*, vol. 3, 1989, 1540–1543.

[7] Krishnapuram, B., Sichina, J., and Carin, L.
Integrated design of synthetic aperture radars for unmanned aircraft.
IEEE Sensors Journal, **3**, 2 (Apr. 2003), 147–157.

[8] Jakowatz, C. V., Jr., Wahl, D. E., Eichel, P. H., Ghiglia, D. C., and Thompson, P. A.
Spotlight-Mode Synthetic Aperture Radar: A Signal Processing Approach.
Boston, MA: Kluwer, 1996.

[9] Gini, F., Lombardi, F., and Montanari, M.
Layover solution in multibaseline SAR interferometry.
IEEE Transactions on Aerospace and Electronic Systems, **38**, 4 (2002), 1344–1356.

[10] Lombardi, F., Gini, F., and Matteucci, P.
Application of array processing techniques to multibaseline InSAR for layover solution.
In *Proceedings of IEEE Radar Conference*, 2001, 210–215.

[11] Desai, M. D.
Spotlight mode SAR stereo technique for height computation.
IEEE Transactions on Image Processing, **6**, 10 (1997), 1400–1411.

[12] Seymour, M. S., and Cumming, I. G.
Maximum likelihood estimation for SAR interferometry.
In *Proceedings of Geoscience and Remote Sensing Symposium*, 1994, 2272–2275.

[13] Peebles, P. Z.
Radar Principles.
New York: Wiley, 1998.

[14] Li, J., Bi, Z., Liu, Z., and Knaell, K.
Use of curvilinear SAR for three-dimensional target feature extraction.
IEE Proceedings of Radar, Sonar and Navigation, **144**, 5 (Oct. 1997), 275–283.

[15] Cramér, H.
Mathematical Methods of Statistics.
Princeton, NJ: Princeton University Press, 1946.

[16] Linnehan, R., Schindler, J., Perlovsky, L., Rangaswamy, M., and Brady, D.
Phenomenology-based waveform design using Cramér Rao theory.
In *Proceedings of IEE Waveform Diversity and Design Symposium*, Nov. 2004.

[17] Soumekh, M.
Synthetic Aperture Radar Signal Processing with Matlab Algorithms.
New York: Wiley, 1999.

[18] Scharf, L. L.
Statistical Signal Processing.
Reading, MA: Addison-Wesley, 1991.

[19] Van Trees, H. L.
Detection, Estimation and Modulation Theory.
New York: Wiley, 1968.

[20] Helstrom, C. W.
Elements of Signal Detection and Estimation.
Englewood Cliffs, NJ: Prentice-Hall, 1995.

[21] Stoica, P., and Moses, R. L.
Introduction to Spectral Analysis.
Englewood Cliffs, NJ: Prentice-Hall, 1997.

[22] Gini, F.
Estimation strategies in the presence of nuisance parameters.
Signal Processing (the Netherlands).
55, 2 (1996), 241–246.

[23] Swokowski, E. W.
Calculus (5th ed.).
Boston, MA: PWS-Kent, 1991.

[24] Perlovsky, L. I.
Cramer-Rao bound for tracking in clutter and tracking multiple objects.
Pattern Recognition Letters, **18**, 3 (1997), 283–288.

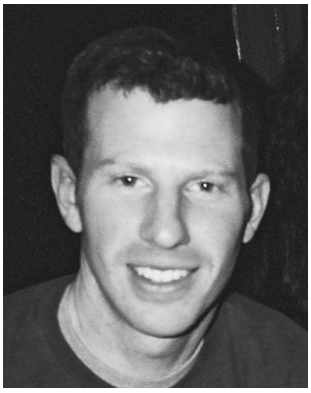

Robert Linnehan (S'01) received the B.E.E. degree from The Catholic University of America, Washington, D.C., in 1996 and the M.S.E.E. degree from Northeastern University, Boston, MA, in 2002.

Currently he works for the Air Force Research Laboratory at Hanscom AFB, MA, and is completing the Ph.D. degree in electrical engineering from Northeastern University.

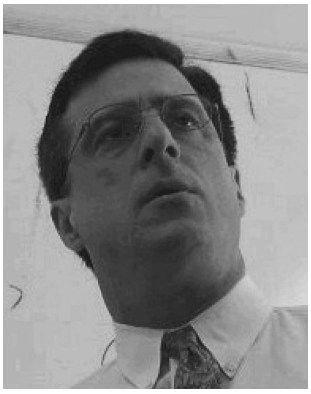

David Brady (M'84) obtained the B.S.E.E. from Carnegie-Mellon University, Pittsburgh, PA, the M.S.E.E. degree from the California Institute of Technology, Pasadena, and the Ph.D.E.E. from Princeton University, Princeton, NJ.

He is currently an associate professor in the ECE Department at Northeastern University and consults for several industrial affiliates. His research interests involve applications of statistical inference to engineering problems, including: multiuser detection, blind source separation, multipath channel characterization, indoor radiolocation, and DNA sequencing algorithms.

John K. Schindler (S'62—M'64—SM'89—F'91) received the S.B. degree from the Massachusetts Institute of Technology, Cambridge, and the M.S. and Ph.D. degrees from Purdue University, Lafayette, IN, all in electrical engineering.

Prior to his retirement, he was the Director of Electromagnetics and Reliability at the Air Force Rome Laboratory where he directed research and development activities in electromagnetics, solid state electronics and reliability. In addition, he served on a defense task force to organize and manage the DoD electronics program. He is a lecturer in electrical engineering at Northeastern University, teaching graduate courses in radar, digital communications and statistical and adaptive signal processing. He has consulted on radar target classification, antenna design and radar cross section measurements. He has been an adjunct professor of electrical engineering at the Air Force Institute of Technology.

Dr. Schindler is a recipient of the IEEE Millennium Medal, the Meritorious Civilian Service Award, and the Presidential Rank Award of Meritorious Executive.

Leonid Perlovsky (M'86—SM'95) is a principal research physicist and technical advisor at the Air Force Research Laboratory. Previously, from 1985 to 1999, he served as chief scientist at Nichols Research, a $0.5 B high-tech organization, leading the corporate research in intelligent systems, neural networks, information science, sensor fusion, and algorithm development. He served as professor at Novosibirsk University and New York University. He participated as a principal in commercial startups developing tools for text understanding, biotechnology, and financial predictions.

Dr. Perlovsky published more than 250 papers, delivered invited keynote plenary talks, tutorial lectures, and authored a book, *Neural Networks and Intellect* (Oxford University Press, 2001) . He organizes conferences on computational intelligence, serves on multiple IEEE committees, Chairs IEEE Boston Computational Intelligence Chapter, and received the Distinguished Member of the IEEE Boston Section Award. He serves as Editor-at-Large for *Natural Computations Journal* and as Editor-in-Chief for *Physics of Life Reviews*.

Muralidhar Rangaswamy (S'89—M'93—SM'98—F'06) received the B.E. degree in electronics engineering from Bangalore University, Bangalore, India, in 1985 and the M.S. and Ph.D. degrees in electrical engineering from Syracuse University, Syracuse, NY, in 1992.

He is presently employed as a senior electronics engineer at the Sensors Directorate of the Air Force Research Laboratory (AFRL), Hanscom Air Force Base, MA. Prior to this he has held industrial and academic appointments. His research interests include radar signal processing, spectrum estimation, modeling non-Gaussian interference phenomena, and statistical communication theory.

Dr. Rangaswamy has coauthored more than 70 refereed journal and conference record papers in the areas of his research interests. Additionally, he is a contributor to 3 books and is a co-inventor on 2 U.S. patents. He is an associate editor for the *IEEE Transactions on Aerospace and Electronic Systems* and is a member of the sensor array and multichannel processing technical committee (SAM-TC) of the IEEE Signal Processing Society. He was a coinstructor with Dr. W. Melvin for two short courses on space-time adaptive processing for the IEEE Boston section (April 2003) and for the IEEE-AESS Atlanta section at the Southeastern Symposium on System Theory (March 2004). He has served on the organizing committee of numerous IEEE AESS and IEEE Signal Processing Society sponsored conferences. He received the 2004 Fred Nathanson memorial radar award from the IEEE AES Society, the 2006 Distinguished Member award from the IEEE Boston Section, and the Charles Ryan basic research award from the Sensors Directorate of AFRL, in addition to 20 AFRL scientific achievement awards.